INTERFACE

royalsocietypublishing.org/journal/rsif

Research



Cite this article: Zhang B, Baskota B, Anderson PSL. 2024 Being thin-skinned can still reduce damage from dynamic puncture. *J. R. Soc. Interface* **21**: 20240311.

https://doi.org/10.1098/rsif.2024.0311

Received: 8 May 2024 Accepted: 29 August 2024

Subject Category:

Life Sciences—Engineering interface

Subject Areas:

biomechanics, biomaterials

Keywords:

layered materials, skin, biological puncture, dynamic, damage resistance

Authors for correspondence:

Bingyang Zhang

e-mails: bz364@cornell.edu; bzhang53@illinois.edu

Philip S. L. Anderson

e-mail: andersps@illinois.edu

Electronic supplementary material is available online at https://doi.org/10.6084/m9.figshare.c.7443052.

THE ROYAL SOCIETY

Being thin-skinned can still reduce damage from dynamic puncture

Bingyang Zhang, Bishal Baskota and Philip S. L. Anderson

Department of Evolution, Ecology, and Behavior, School of Integrative Biology, University of Illinois Urbana-Champaign, 505 S. Goodwin Avenue, Urbana, IL 61801, USA

D BZ, 0000-0003-2138-1191; PSLA, 0000-0001-7133-8322

The integumentary system in animals serves as an important line of defence against physiological and mechanical external forces. Over time, integuments have evolved layered structures (scales, cuticle and skin) with high toughness and strength to resist damage and prevent wound expansion. While previous studies have examined their defensive performance under low-rate conditions, the failure response and damage resistance of these thin layers under dynamic biological puncture remain underexplored. Here, we utilize a novel experimental framework to investigate the mechanics of dynamic puncture in both bilayer structures of synthetic tissue-mimicking composite materials and natural skin tissues. Our findings reveal the remarkable efficiency of a thin outer skin layer in reducing the overall extent of dynamic puncture damage. This enhanced damage resistance is governed by interlayer properties through puncture energetics and diminishes in strength at higher puncture rates due to rate-dependent effects in silicone tissue simulants. In addition, natural skin tissues exhibit unique material properties and failure behaviours, leading to superior damage reduction capability compared with synthetic counterparts. These findings contribute to a deeper understanding of the inherent biomechanical complexity of biological puncture systems with layered composite material structures. They lay the groundwork for future comparative studies and bio-inspired applications.

1. Introduction

The integument of an animal (skin, scales, cuticle and keratinized armours) is the first line of mechanical defence between the organism and the outside world. Surprisingly, this outer layer of tissue is often thin compared with the subcutaneous tissue [1], and, in the case of the skin, it would seem to have a limited contribution to overall mechanical and damage resistance. However, extensive studies have shown unique mechanical and failure behaviours of layered skin and skin-like tissues, with a focus on their remarkable performance in providing protection and resistance against damage and injuries caused by external mechanical hazards such as biting, piercing, insertion and cutting of animal weapons [2–12]. Many of these damage mechanisms can be broadly categorized as puncture and often involve dynamic mechanical interactions and energy transfer processes [13].

Most experimental investigations of the mechanics of puncture in skin, skin-like tissues and tissue-mimicking simulants have been conducted under a low to quasi-static loading rate condition (1×10^{-6} – 1×10^{-2} m s⁻¹) using methods such as deep indentation or needle insertion [2–6,9,11,14,15]. These studies have demonstrated that the layered structure of skin-like materials significantly enhances puncture resistance by redistributing stress and dissipating energy, thereby increasing the force and energy required for puncture and preventing deep penetration and extensive damage. However, natural mechanical interactions, impacts and punctures often occur

at dynamic speeds [13,16–19]. For example, animal weapons and puncture tools have a range of operating speeds, from viper strikes (approx. 3 m s⁻¹) [20–22] to cone snail harpoons (approx. 19 m s⁻¹) [23], cnidarians stinging cells (approx. 30 m s⁻¹) [24] and trap-jaw ant mandibles (approx. 60 m s⁻¹) [25]. A better understanding of puncture behaviours under these biologically relevant dynamic conditions is crucial to gain insight into the evolution and diversification of natural puncture and defensive systems. Dynamic puncture with a conical tool has been reported, in contrast to lower rate puncture, to exhibit distinct damage morphology [26], reduced sensitivity to failure geometry [19] and other unique properties, such as limited maximum puncture performance at higher puncture speeds, related to dynamic energy and momentum transfer [17,27] in viscoelastic rate-dependent target materials. However, a systematic quantification is necessary to explore how a layered skin-like composite material structure mechanically responds to dynamic puncture, and how it attenuates the damage induced to enhance the overall puncture resistance through complex tool–material interactions, energy transfer and rate-dependent effect.

1.1. Theoretical framework and hypotheses

We explore the dynamic puncture mechanics of layered composite materials in both biological (layered porcine skin-adipose tissues) and synthetic (bilayer silicone tissue simulants) model material systems. Based on a theoretical framework of the energetics of dynamic puncture and fracture-relevant material properties, we propose four main hypotheses underlying the puncture resistance and damage reduction capability of a simplified bilayer composite structure consisting of a thin skin-like layer that covers a soft substrate.

In a general context, one of our main hypotheses is that differences in material properties between the outer skin-like layer and the substrate layer play an important role in enhancing the overall puncture resistance and damage reduction capability of the composite material. An outer layer material having higher stiffness and toughness compared with the substrate material will potentially lead to enhanced energy dissipation via higher stored elastic energy and work to fracture per unit thickness of penetration and thus reduce the overall extent of damage along the puncture direction. This shielding effect can be further enhanced by friction and viscosity or by an increase in the thickness of the outer skin-like layer, based on the hypotheses in our following discussions. Consequently, such a bilayer structure would produce a smaller-scale puncture damage than the substrate material alone for the same initial energy investment. Theoretically, this damage reduction capability can be explained by the previously established model for the energetics of dynamic puncture by Zhang & Anderson [13], where the total energy required for a dynamic puncture event with a conical tool, or the loss of initial kinetic energy, W_k , scales with the maximum depth of puncture D_{max} in the following generalized relationship:

$$W_k = k_{\text{frac}} \Gamma D_{\text{max}}^2 + k_e \mu D_{\text{max}}^3 + k_f f D_{\text{max}}^3$$
 (1.1)

where the three terms represent energy contributions from creating fracture surfaces, elastic deformation and frictional dissipation, respectively. $k_{\rm frac}$, k_e and k_f are the corresponding pre-factors related to the half angles of the puncture tool $(\theta_{\rm tool})$ and fracture $(\theta_{\rm frac})$, with explicit expressions given in Zhang & Anderson [13]. Specifically, $A_{\rm frac} = k_{\rm frac} D_{\rm max}^2 \approx \tan \theta_{\rm frac} D_{\rm max}^2$ estimates the area of the fracture surface. Γ is the fracture toughness/critical strain energy release rate, μ is the shear modulus and $f = \eta p$ is a frictional constant calculated as the product of the Coulomb friction coefficient (η) and the interfacial contact pressure (p) [13]. Equation (1.1) implies that for the same amount of initial energy investment, W_k , a higher value of Γ or μ will lead to a decreased $D_{\rm max}$. Conversely, for a fixed penetration distance, such as a controlled outer layer thickness $(t_{\rm out})$, higher stiffness and toughness (i.e. μ and Γ) will result in larger energy dissipation and thus less energy available for further penetration in the substrate. Both cases contribute to an overall increase in puncture resistance and a reduction in damage size in the bilayer composite material.

Following from the above-mentioned energetics, another important hypothesis is that the longitudinal extent of puncture damage or the maximum depth of puncture (D_{max}) decreases asymptotically at larger outer layer thicknesses (t_{out}), and its magnitude is constrained by the properties of the two material layers. To show this via puncture energetics, we assume an infinitely large bilayer structure with a half-space of substrate material covered by an outer layer (electronic supplementary material, figure S1). An incremental increase in outer layer thickness (Δt_{out}) substitutes a section of the original damage (ΔD_{max}) in the substrate with new damage in the outer layer, following an energy balance,

$$W_{k} = W_{\text{out}}(t_{\text{out},0} + \Delta t_{\text{out}}) + W_{\text{sub}}(D_{\text{max},0} - \Delta D_{\text{max}} - t_{\text{out},0})$$

$$= W_{\text{out}}(t_{\text{out},0}) + W_{\text{sub}}(D_{\text{max},0} - t_{\text{out},0}), \tag{1.2}$$

where $t_{\text{out,0}}$ and $D_{\text{max,0}}$ are the original thickness of the outer layer and total depth of puncture, respectively; W_{out} and W_{sub} are the energy contributions from the outer and substrate layers, respectively. W_{sub} takes a form similar to equation (1.1) with the substitution of damage size and material properties ($W_{\text{sub}} = W_k$). The magnitude of W_{out} for a thickness t_{out} can be approximated using the following expression (see the electronic supplementary material for the detailed deviation):

$$W_{\text{out}}(t_{\text{out}}) \approx W_k \left(\frac{A_{\text{out}}}{d_0 - d_I} + \frac{1}{2} t_{\text{out}} \right) - W_k \left(\frac{A_{\text{out}}}{d_0 - d_I} - \frac{1}{2} t_{\text{out}} \right), \tag{1.3}$$

where $A_{\text{out}} \approx \frac{1}{2}(d_0 + d_I)t_{\text{out}}$ calculates the area of fracture surface in the outer layer, and d_0 and d_I denote the width of the fracture surface at the surface and interface, respectively (electronic supplementary material, figure S1). The relative magnitude of the new total depth of puncture characterizes the damage reduction capability of the bilayer structure and can be calculated by

solving for ΔD_{max} and using the expression $D_{\text{norm}} = D_{\text{max}}/D_{\text{max},0} = 1 - (\Delta D_{\text{max}} - \Delta t_{\text{out}})/D_{\text{max},0}$. Equations (1.2) and (1.3) lead to several important predictions that can be validated through puncture experiments in bilayer model materials:

- For the extent of damage (D_{max}) to decrease with increasing t_{out} , ΔD_{max} must be greater than Δt_{out} , which requires the outer layer to have stronger energy dissipation capability than the substrate material.
- Interlayer differences in fracture morphology, such as a larger area of fracture surface (A_{out}) or lateral extent of damage (d_0 and d_I) due to a more brittle failure behaviour in the outer layer compared with the substrate layer, also lead to higher energy dissipation and a stronger damage reduction capability.
- As t_{out} increases, at a critical point when $D_{\text{max}} = t_{\text{out}}$, dynamic puncture no longer penetrates and reaches the substrate layer, and the outer layer encompasses the entire fracture surface. Consequently, the upper limit of D_{max} is determined by the less damage-resistant substrate material; D_{max} decreases and eventually approaches its lowest possible value, constrained by the properties of the outer layer material, as t_{out} increases.

A further observation from the above-mentioned energy balance is that the substrate material also plays a substantial role in damage reduction. Therefore, we hypothesize that when the magnitude of damage reduction (ΔD_{max}) due to an increase in the thickness of the outer layer (Δt_{out}) compensates for the difference between the initial extent of damage ($D_{\text{max},0}$) in different types of substrate materials (e.g. a moderate resistance silicone (MRS) elastomer and an ultra-soft silicone (USS) elastomer, see §2 for details), i.e.

$$\left(\frac{\Delta D_{\text{max}}}{D_{\text{max},0}}\right)_{\text{USS}} > \left(\frac{\Delta D_{\text{max}}}{D_{\text{max},0}}\right)_{\text{MRS}},$$
(1.4)

a lower magnitude of D_{norm} is obtained for the bilayer tissue simulant having a softer, less damage-resistant substrate layer (e.g. USS). This implies a higher damage reduction capability for a larger difference between the outer and substrate layers, consistent with our first hypothesis. Nevertheless, we speculate that the measured values of D_{max} from the two types of bilayer silicone tissue simulants will eventually asymptote to a similar lower limit if a thicker outer layer is applied.

Based on the viscoelastic behaviours of constituent materials, we further hypothesize a strong rate dependence of fracture-relevant material properties in both our selected bilayer silicone tissue simulants and natural skin tissues that may significantly impact their capability to resist puncture damage. Experimental evidence has shown that soft elastomers generally exhibit increased elastic modulus and fracture toughness at higher applied strain rates [28–32]. Similar rate-based stiffening and toughening effects have been reported in both natural adipose [33] and skin tissues [28,34–36]. We consider a case where the magnitude of changes in material properties is significantly larger in the substrate material of a bilayer composite structure than in the outer layer material for the same increase in the applied puncture rate (v). Consequently, the difference between the two layers diminishes at higher puncture rates. Based on the energy balance described in equations (1.1) and (1.2), the resultant puncture damage becomes less sensitive to the bilayer structure ($t_{\rm out}$) as the energy dissipation and damage reduction capabilities of the two layers approach (i.e. $W_{\rm sub} \rightarrow W_{\rm out}$). Within silicone-based tissue simulants, such a rate-based effect can be induced by a lower level of chemical cross-linking in the substrate material [37–41], which introduces more free polymer chains and defects into the network [41,42] and results in lower stiffness. All of these factors lead to an enhanced viscoelastic effect [31] and, consequently, stronger rate dependence of toughness and modulus in the substrate material. However, we note that complex natural layered materials, such as the selected porcine skin-adipose tissues, may exhibit a unique viscoelastic effect and different rate-based puncture response than these synthetic counterparts, which necessitates further quantification.

To test the above-mentioned hypotheses that the effects of interlayer material properties, outer layer thickness and dynamic puncture rate play a significant role in enhancing the overall puncture resistance and damage reduction capability of bilayer composite materials, we perform dynamic puncture tests in both natural skin tissues and synthetic tissue simulants. As described in §2, the puncture-relevant material properties, such as stiffness and fracture toughness, outer layer thickness and puncture rate conditions, are carefully tuned in the bilayer tissue simulants to partly reproduce the properties of natural skin tissues and enable a quantitative comparison of their puncture behaviours. This provides a fundamental material and mechanical basis for examining the hypotheses (§3). We discuss the mechanics underlying the distinct fracture morphology, extent of damage, puncture resistance, and rate dependence of natural and synthetic layered materials, and specifically how similarities and differences in their material properties are mechanically related to and influence these different aspects of dynamic puncture behaviours. This systematic comparative characterization provides experimental evidence for the generalization of the above-mentioned theoretical framework to explain the damage reduction capability of bilayer skin-like structures.

2. Methods

Downloaded from https://royalsocietypublishing.org/ on 20 January 2025

2.1. Porcine skin-adipose tissues

Pork jowls were obtained from the Meat Science Laboratory at the University of Illinois Urbana-Champaign (Urbana, IL, USA) and subjected to freezing within a time frame of 1 h. The jowls were kept frozen for approximately 24 h before sample preparation. The jowls were then thawed for approximately 3 h to allow adequate softening and cut into layered cubic samples (figure 1f,i) weighing approximately 90 g each using a sharp fillet knife. Although the muscle layer of a sample was not punctured

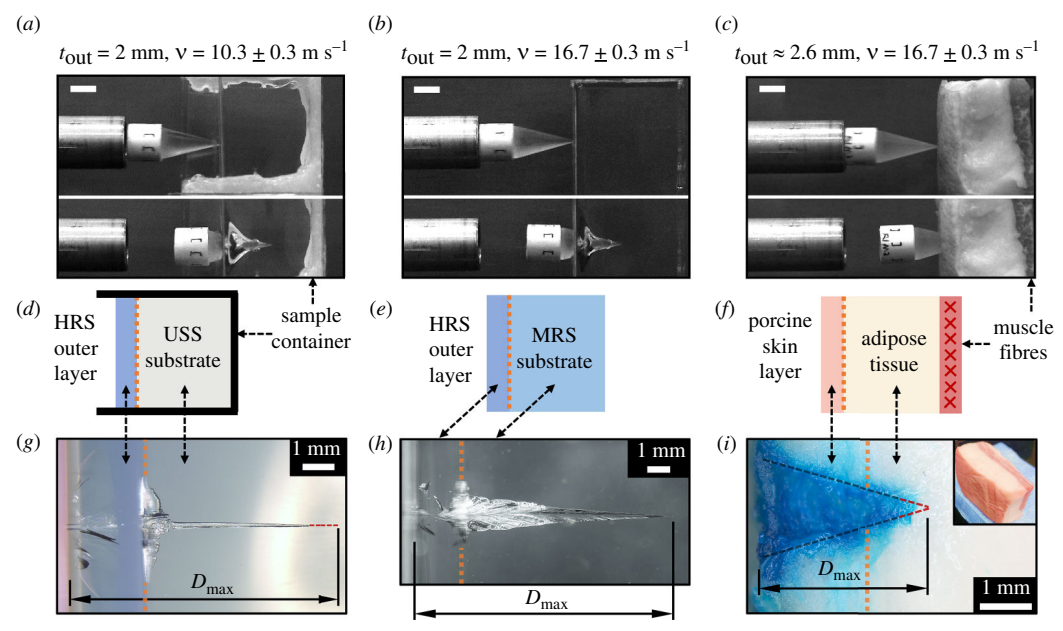


Figure 1. Representative dynamic puncture testing systems and resultant damage morphologies. Selected layered composite material samples and test conditions: left column: bilayer silicone tissue simulant with a high resistance silicone (HRS) outer layer and an ultra-soft silicone (USS) substrate ($t_{out} = 2 \text{ mm}$, $v = 10.3 \pm 0.3 \text{ m s}^{-1}$); middle column: bilayer silicone tissue simulant with an HRS outer layer and a moderate resistance silicone (MRS) substrate ($t_{out} = 2 \text{ mm}$, $v = 16.7 \pm 0.3 \text{ m s}^{-1}$); right column: layered porcine skin-adipose tissue ($t_{out} \approx 2.6 \text{ mm}$, $v = 16.7 \pm 0.3 \text{ m s}^{-1}$). See table 1 for detailed material properties relevant to puncture. (a–c) Still-frame high-speed images of dynamic puncture tests captured at the onset of impact (upper) and maximum penetration (lower), respectively. Scale bars: 10 mm. (d–f) Schematics of the synthetic and biological layered structures. (g–i) Microscopic images of undeformed fracture surfaces. The orange dotted lines indicate the interface between the outer and substrate layers. (i) The fracture surface in a porcine sample was dyed with blue food colouring before being cross-sectioned to increase the visibility and contrast with surrounding tissues. The vertex of the fracture surface in (g) and (i) is determined by identifying and extrapolating the edge lines (as indicated by dashed lines of different colours). Inset of (i): image of the porcine sample before puncture.

during the test, the sample preparation ensured that the muscle fibres were orthogonally oriented to the puncture direction (figure 1f) to promote uniformity. The samples were tested in a 1 h time window after the thawing and cutting processes. Due to time constraints, a subset of the prepared samples was refrozen before testing, and their results were examined for consistency and included in the final analysis.

2.2. Bilayer silicone tissue simulants

Different silicone elastomers were selected to create transparent bilayer composite material structures as skin-mimicking tissue simulants. These tissue simulants consist of an outer layer and a substrate layer with controlled but markedly different thicknesses, elastic moduli, fracture toughness and stretchability, which partly reproduce the structures and material properties of porcine skin-adipose tissues. These tailored material characteristics enable a systematic evaluation of distinct puncture behaviours and fracture morphologies between the two layers, as well as between the two selected types of substrate materials, compared with those in porcine skin-adipose tissues. This allows for testing the hypotheses described in §1, particularly regarding how the effects of interlayer properties and outer layer thickness impact the damage reduction capability.

Fabrication of bilayer silicone tissue simulants was carried out by adapting established protocols [13,19,43], which involved a two-step curing process. The substrate layer material was fabricated using Solaris silicone (Smooth-On, Inc.) or Sylgard 184 silicone (Dow Corning, Inc.) by mixing two parts of the polymer kit as received in a 1:1 (weight by weight (w/w)) mixing ratio (Solaris), designated as a MRS substrate, or 55:1 (w/w) mixing ratio (Sylgard 184), designated as an USS substrate. These designations reflect the mechanical characteristics and functions of the materials during puncture tests. The mixture was subsequently degassed (approx. 30 min), poured into a cube mould, cured and placed at room temperature for approximately 24 h. A standard cube mould (ASTM C-109) was used for the MRS substrate material with polycarbonate (PC) sheets (0.02 inches thick) attached to the inner surfaces to enhance the clarity and transparency of the samples. A customized cube container (figure 1) constructed with the same PC sheets was used for the USS substrate material to account for its strong adhesion and low modulus. Subsequently, an outer skin-like layer is fabricated by mixing part A and part B Solaris silicone polymers in a ratio of 4:1 (w/w), designated as a high resistance silicone (HRS) outer layer. The liquid mixture was degassed, poured on top of the substrate layer at a designed weight (2 or 4 g) and cured (approx. 24 h) to create an outer layer with a controlled thickness (2 or 4 mm). The sample cubes were examined before testing for proper dimensions (approx. $49 \times 49 \times 42$ mm, $t \times w \times h$) and mass verification (approx. 100 ± 1 g).

In table 1, we compare documented values of selected material properties, including shear modulus (μ), fracture toughness/critical strain energy release rate (Γ) and tensile stretchability (λ^*), between silicone simulant materials and porcine skin and adipose tissues. Although the bilayer silicone simulant structures used in this study (figure 1) are a simplified representation of the anatomy of animal skin [50], their constituent materials are suitable model systems for studying the mechanical behaviours of skin tissues due to their high controllability and low variability in material properties and structures [11,50–52].

Notably, the design of our bilayer silicone simulant integrating a USS substrate reproduces the stiffness of porcine skin and adipose tissues, providing a basis for the comparison between synthetic and biological layered materials. Specifically, the HRS outer layer has a documented low-rate shear modulus, $\mu \approx 390$ kPa [43], which coincides with $\mu \approx 400$ kPa measured from porcine skin using low-rate uniaxial tension [28]. The USS substrate material and silicone elastomers with similar polymer–cross-linker mixing ratios have been widely used for their extremely low modulus and biocompatibility [11,41,42,45,46]. Compared with biological materials, the low-rate shear modulus of the USS substrate ($\mu \approx 5$ kPa) [11,45,46] closely matches $\mu \approx 5.6$ kPa determined from porcine subcutaneous adipose tissues using low-frequency shear rheology (approx. 0.1 rad s⁻¹) [47] and agrees in order of magnitude with other reported values ($\mu \approx 1$ kPa) [33,53]. In comparison, the MRS substrate layer exhibits an intermediate shear modulus (table 1). However, the strong viscoelastic behaviours of the MRS substrate, evident from previous high-rate puncture tests [19,26], allow us to test the hypothesis on the rate-based puncture resistance of layered composite materials.

Despite successfully replicating elastic moduli, the different toughness values in table 1 suggest that the bilayer simulant with a USS substrate and its tissue counterpart may still exhibit divergent failure behaviours during dynamic puncture. Notably, the fracture toughness of porcine skin ($\Gamma \approx 30 \text{ kJ m}^{-2}$) estimated using mode-I quasi-static crack opening tests [44] is two orders of magnitude higher than $\Gamma \approx 0.18 \text{ kJ m}^{-2}$ for the HRS outer layer material measured from pure shear tearing tests at a quasi-static rate [43,54]. While the failure properties of the USS elastomer are practically challenging to measure due to its softness and strong adhesion [42,45], it is unlikely to be tougher than porcine subcutaneous tissue, considering an order-of-magnitude estimation of the puncture toughness of USS substrates ($\Gamma \approx 0.1 \text{ kJ m}^{-2}$) from low-rate puncture tests using specific tool and failure geometries [11]. In contrast, porcine adipose tissue exhibits $\Gamma \approx 4 \text{ kJ m}^{-2}$ estimated from low-rate trousers tests [48], which is even higher than $\Gamma \approx 0.18 \text{ kJ m}^{-2}$ of the HRS outer layer. Given these differences in toughness, the skin-mimicking tissue simulant probably underestimates the puncture resistance, resulting in a different extent and morphology of damage compared with the natural skin tissue.

2.3. Dynamic puncture method

Dynamic puncture tests were performed using an established experimental framework [13,19] integrating a compressed air cannon (Ballistic Loading and Structural Testing Lab; NC State University) and three-dimensional (3D)-printed projectiles/puncture tools (Form 3 stereolithography (SLA) 3D printer, Formlabs Inc., clear resin, FLGPCL04). The rates of dynamic puncture ($v = (10.3 \pm 0.3, 16.7 \pm 0.3, 34.4 \pm 0.8)$ m s⁻¹; numbers indicate the mean and s.d.) were controlled by the pressure and loading position of the projectile inside the air cannon and calibrated using high-speed imaging (FASTCAM SA-Z, Photron Inc.; $10\ 000-20\ 000$ fps) across all samples tested.

The selected puncture tools have a conical shape with a controlled cusp angle, $\theta_{\text{tool}} = 30^{\circ}$, and an average tip radius $r \approx 40 \pm 2 \,\mu\text{m}$ after surface polishing (2000 grit sandpaper). Given the length scale and focus of our puncture experiments on deep penetration of layered materials, we adopted conical geometry as a simplified representation of natural puncture tools. It provides a solid mathematical basis and facilitates comparison with previous studies adopting similar geometry on the biomechanics of puncture [3,55–59]. The choice of the cusp angle corresponds approximately to the average value of a range of tool angles found in nature [19]. We recognize that while a power-law or paraboloid-like geometry is considered representative in nature based on the profile of the tip region (with a length scale of $\lesssim 1$ mm) [60] or growth [61] of various biomechanical elements, it does not preclude the coexistence of a conical shape in the same puncture tool at a larger scale beyond the tip region. While a power-law profile at the tip may play an important role during the damage initiation phase of puncture on the surface of a target material by enhancing the buckling resistance of the tip [60], such effect becomes less significant at a larger depth of puncture during the deep penetration phase. Therefore, the body of a puncture tool, which governs the material interactions during deep penetration [13], can still maintain a conical shape without negatively impacting performance.

2.4. Characterization of fracture surface

Images of the fracture surfaces created by dynamic puncture tests (e.g. figure 1g-i) were captured using a stereo microscope (M205C, Leica Microsystems Inc.). The maximum depth of puncture (D_{max}) defines the distance between the superficial opening and the vertex of the fracture surface along its centreline. The mean and s.d. of D_{max} were determined by summarizing measurements from both post-processing (ImageJ) and manual probing [13,19].

royalsocietypublishing.org/journal/rsif J. R. Soc. Interface 21: 20240311

Downloaded from https://royalsocietypublishing.org/ on 20 January 2025

Table 1. Comparison of documented material properties for silicone simulant materials and porcine tissues.

material name	elastomer	structural role	μ (kPa)	Г (kJ m ⁻²)	λ^*
HRS	Solaris (4 : 1)	outer skin layer	390 [43]	0.18 [43]	2 [43]
porcine skin		outer skin layer	400 [28]	≈30 [44]	1.2–1.8 [28]
MRS	Solaris (1 : 1)	substrate layer	130 [43]	0.05 [43]	2.9 [43]
USS	Sylgard 184 (55 : 1)	substrate layer	5 [11,45,46]	≈0.1 [11]	≳4 [11,26,42]
porcine adipose	_	substrate layer	5.6 [47]	4 [48]	1.3 [33,49]

Symbols: μ , shear modulus; Γ , fracture toughness; λ^* , tensile stretchability.

2.5. Statistical analysis

The statistical significance of all datasets was quantified using a two-way analysis of variance (ANOVA) in Matlab (figures 2 and 3b). The resultant p-values are denoted in the corresponding figures with asterisks (p < 0.05: *; p < 0.01: ***; p < 0.001: ***) and included in their captions.

3. Results and discussion

3.1. Comparison of dynamic puncture behaviours for natural tissues and tissue simulants

3.1.1. Puncture damage morphology

Representative images of puncture damage in figure 1 demonstrate distinct fracture morphologies in bilayer silicone tissue simulants and porcine skin-adipose tissues. The fracture surfaces created by dynamic conical puncture exhibit a clear transition between the outer and substrate layers in both types of bilayer silicone tissue simulants (e.g. figure 1g,h). The HRS outer layer exhibits a planar penny-shaped crack characterized by a large lateral extent of damage, which is estimated to be similar to the corresponding width/diameter of the puncture tool (see electronic supplementary material). This corresponds to a brittle type of puncture failure behaviour [43,51]. Consequently, the area of the fracture surface in the outer layer (i.e. A_{out} in equation (1.3)) is substantially increased compared with in the substrate layer. As shown in figure 3, a significant reduction in damage $(\Delta D_{\text{norm}} \approx 20\%)$ occurs with a small outer layer thickness ($t_{\text{out}} = 2$ mm). This damage reduction capability is contributed by the extra energy dissipation from the increased fracture surface area (A_{out}) in the thinner outer layer, in addition to the contributions of higher stiffness (μ) and toughness (Γ). This is consistent with the correlation between A_{out} and D_{max} in equation (1.3) and is confirmed by the theoretical predictions in figure 3.

Moreover, we expect the contribution to energy dissipation due to friction and viscosity to decrease with a thicker and more brittle outer layer. As shown in Fregonese & Bacca and Montanari & Spagnoli [62,63], both the average contact pressure and contact area will decrease significantly for a larger lateral extent of damage relative to the tool diameter, due to the detachment of the fracture surface from the tool surface. However, such a decrease in energy dissipation may not offset the increase in the fracture or elastic energy contribution due to higher A_{out} , μ and Γ , as suggested by figure 3. Future quantitative verification requires an accurate estimation of the tool–material contact area in the outer layer, which may be complicated by partial visibility of the closed transparent fracture surfaces (e.g. figure 1g,h).

In contrast, both the MRS and USS substrates exhibit a planar crack with a regular triangular shape, consistent with the ductile-like puncture failure behaviour prevailing in soft and stretchable materials [13,26,64]. This damage morphology indicates a fully expanded material cavity conforming to the surface of the puncture tool during deep penetration. The interlayer transition of puncture failure behaviour from brittle to ductile, as pointed out by Zhang & Anderson [13,26], is primarily governed by the defect/flaw tolerance and the strength of the crack-blunting effect of the target material, which determines the deformability of the puncture cavity and thus damage morphology. It can be contributed by a material's low stiffness and high stretchability [65]. As listed in table 1, this is supported by the relatively low shear modulus ($\mu \approx 130$ kPa) and high tensile stretch at break ($\lambda^* \approx 2.9$) for the MRS substrate layer and $\mu \approx 5$ kPa and $\lambda^* \gtrsim 4$ for the USS substrate layer, compared with $\mu \approx 390$ kPa and $\lambda^* \approx 2$ for the HRS outer layer at low rates.

The ductile puncture behaviour in the substrate layer leads to the following two interesting observations related to the extent of damage: (i) the longitudinal extent/total length of damage in the undeformed state (D_{max}) is similar to the length of the region of the puncture tool that penetrates the composite material and (ii) the lateral extent/width of damage in the undeformed substrate layer is significantly smaller than the corresponding width/diameter of the puncture tool, and the relative magnitude of the extent of damage does not change within the same substrate material. Both observations are evident from previous dynamic puncture tests in MRS and USS materials [13,26] and can be verified from figure 1 through measurements. In particular, the angular ratio between the tangent of the half cusp angle of the puncture tool and that of the undeformed damage is a constant that mathematically corresponds to the stretchability of the target material at a specific applied rate of puncture

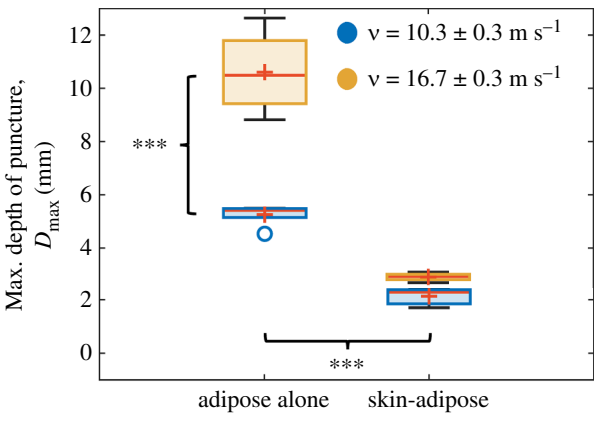


Figure 2. Box and whisker plot of the dynamic puncture results of porcine tissues. The datasets were obtained from both layered porcine skin-adipose tissues ('skin-adipose') and adipose tissues with skin removed ('adipose alone') at two different puncture rates ($v = 10.3 \pm 0.3$ m s⁻¹ and $v = 16.7 \pm 0.3$ m s⁻¹). The top and bottom edges of each box correspond to the 75th and 25th percentiles; the centre red line indicates the median; and the red cross indicates the average. The whiskers indicate the scatter of the dataset, with the outliers marked by open circles. Statistical analysis using two-way ANOVA indicates a significant effect of skin layer (horizontal variation, bottom asterisks (***): p < 0.001) and a significant effect of puncture rate (vertical variation, left asterisks (***): p < 0.001) on the damage reduction capability.

[26] (i.e. $\tan \theta_{tool}/\tan \theta_{frac} \approx \lambda^*$). Therefore, the high stretchability of the two substrate materials explains their small lateral extent of damage.

In contrast to the interlayer transition observed in silicone tissue simulants, the puncture damage in cross-sectioned porcine skin-adipose tissue samples exhibits an overall triangular shape similar in both undeformed layers. The interlayer disruption to the crack shape is negligible at $v = 16.7 \pm 0.3$ m s⁻¹ (figure 1i), while no penetration through the skin layer occurs at $v = 10.3 \pm 0.3$ m s⁻¹. Within all porcine tissue samples tested, the lateral extent/angle of the undeformed fracture surface is comparable to or slightly smaller than the corresponding diameter of the puncture tool throughout the entire depth of puncture, indicating a ductile puncture failure behaviour in both skin and adipose layers similar to that observed in silicone tissue simulants. This is further evidenced by our observation during and immediately after dynamic puncture that the displaced tissue conforms to the surface of the puncture tool, and no brittle lateral crack expansion occurs in the porcine tissue samples. It is interesting to note that the angular ratio in porcine skin and adipose tissues is consistent with a range of their stretchability determined from low-rate uniaxial tension tests [28,33,49], $\lambda^* \approx 1.2-1.8$ (table 1), which is even lower than that of the HRS outer layer material. While these observations seem to contradict the observed ductile puncture response, we emphasize that high stretchability is not a necessary condition for high defect/flaw tolerance and strong crack-blunting. As discussed in the next section, porcine skin and adipose tissues possess unique fibrous microstructures that can provide additional reinforcement and fundamentally alter their failure behaviour compared with soft polymeric materials. The similarity in the ductile failure behaviour and the stretchability of the outer skin layer and the subcutaneous adipose layer, despite their markedly different stiffness and toughness (table 1), may theoretically play a key role in minimizing cross-layer transition of damage, mitigating excessive lateral crack growth and thus preventing delamination as observed in tissue simulant counterparts.

3.1.2. Resistance to dynamic puncture

Downloaded from https://royalsocietypublishing.org/ on 20 January 2025

In addition to damage morphology, the resistance to puncture damage, evaluated by the average maximum depth of puncture (D_{max}) and D_{norm} , shows some level of similarity in the dependence on the outer layer but differs significantly in magnitude and rate dependence between the natural skin tissues and synthetic bilayer tissue simulants.

The box and whisker plot in figure 2 compares D_{max} measured from two types of porcine samples (bilayer skin-adipose tissue and single-layer adipose tissue with skin layer removed) under two selected puncture rates ($v = 10.3 \pm 0.3$ m s⁻¹ and $v = 16.7 \pm 0.3$ m s⁻¹). The presence of the porcine skin layer markedly enhances puncture resistance at both dynamic puncture rates, as indicated by the significantly reduced D_{max} values in bilayer porcine samples compared with adipose tissue samples (two-way ANOVA, p < 0.001). Additionally, the two-way ANOVA reveals a significant effect of puncture rate (v) on D_{max} (p < 0.001), as well as a strong interaction between the effects of the skin layer and v (p < 0.001).

Figure 3 presents the results of the dynamic puncture test for synthetic bilayer tissue simulants (squares and circles). The puncture resistance of each sample is evaluated by the maximum depth of puncture (D_{max}), plotted against the thickness of the corresponding outer layer (tout). Different groups of data in figure 3 indicate variations in puncture rate $(v = (10.3 \pm 0.3, 16.7 \pm 0.3, 34.4 \pm 0.8) \text{ m s}^{-1})$ and material type (bilayer simulant having either a MRS or USS substrate). Figure 3b shows normalized D_{max} values, $D_{\text{norm}} = D_{\text{max}}/D_{\text{max},0}$, where $D_{\text{max},0} = D_{\text{max}}(t_{\text{out}} = 0)$ is the maximum value within the same data group, i.e. the average D_{max} determined from the substrate layer alone. The normalized trends in figure 3b isolate the dependence of the extent of damage on tout from the magnitude effect. As indicated in figure 3b, a two-way ANOVA yields statistically significant dependence (p < 0.001) of D_{norm} on both t_{out} and v in bilayer silicone samples having an MRS substrate. Furthermore, a significant interaction between t_{out} and v (p < 0.05) indicates that the effect of t_{out} depends on applied v.

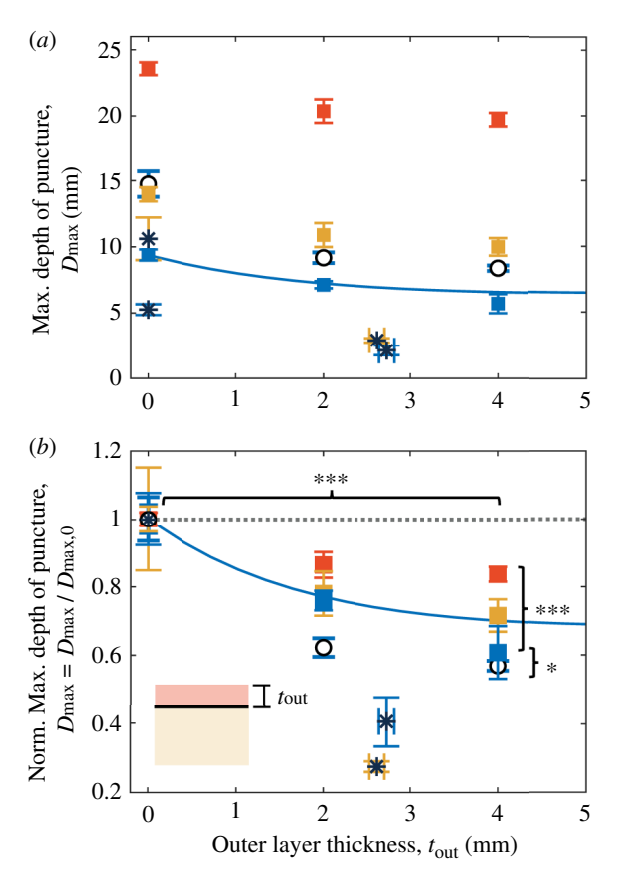


Figure 3. Puncture performance in different layered composite materials. Data were obtained from both bilayer silicone simulant samples (MRS substrate: solid squares; USS substrate: open circles) and porcine skin-adipose tissue samples (stars) at different outer layer thicknesses ($t_{out} = 0-4$ mm) and puncture rates ($v = 10.3 \pm 0.3$ m s⁻¹: light blue error bars, $v = 16.7 \pm 0.3$ m s⁻¹: yellow error bars, $v = 34.4 \pm 0.8$ m s⁻¹: orange error bars). (a) The dependence of the maximum depth of puncture (D_{max}) on t_{out} and v. (b) The dependence of relative damage reduction capability, as evaluated by the normalized maximum depth of puncture values ($D_{norm} = D_{max}/D_{max}$, D_{max} ,

Downloaded from https://royalsocietypublishing.org/ on 20 January 2025

Similarly, a two-way ANOVA between the data of the two types of silicone samples (MRS and USS substrates) indicates statistically significant effects of substrate material (p < 0.05) on the damage reduction capability (D_{norm}). These observations are consistent with the dependence of puncture damage reduction on t_{out} , v and the substrate material predicted by the hypotheses in \$1

To quantitatively compare the puncture resistance and damage reduction capability in natural tissues and tissue simulants, the D_{max} and D_{norm} values of porcine skin-adipose tissue samples are included in figure 3, where the t_{out} values correspond to the average thickness of the skin layer measured across all porcine skin-adipose samples. While the lower D_{max} values in the porcine adipose tissue alone compared with its silicone substrate counterparts (USS and MRS; figure 3) already indicate a higher damage resistance, incorporation of the skin layer provides porcine tissue with even stronger reinforcement compared with the silicone outer layer counterpart. Despite having a relatively low skin layer thickness ($t_{\text{out}} \approx 2.7 \text{ mm}$), the porcine skin-adipose tissue samples exhibit average relative magnitudes of damage, $D_{\text{norm}} \approx 0.40$ at $v = 10.3 \pm 0.3 \text{ m s}^{-1}$ and $D_{\text{norm}} \approx 0.27 \text{ at } v = 16.7 \pm 0.3 \text{ m s}^{-1}$, which are even lower than the average values of D_{norm} obtained from bilayer silicone samples with $t_{\text{out}} = 4 \text{ mm}$ at the corresponding puncture rates.

Additionally, the porcine tissue samples exhibit a stronger damage reduction capability (an approx. 73% decrease in D_{norm}) as the applied puncture rate increases (from $v = 10.3 \pm 0.3$ m s⁻¹ to $v = 16.7 \pm 0.3$ m s⁻¹). This rate dependence contrasts with the diminishing damage reduction capability observed in the bilayer simulants with an MRS substrate at higher rates (figure 3*b*), which might be related to the unique viscoelastic effect of skin and adipose tissues, such as a strong strain-rate-based stiffening

effect [28,49,66]. These results highlight distinct dynamic puncture response and remarkable rate-mediated puncture resistance of porcine skin-adipose tissues compared with their synthetic counterparts, despite their similarity in elastic moduli. Further considerations are necessary to account for the intrinsic mechanical and microstructural complexity of layered skin tissues.

For example, the enhanced damage reduction capability of the porcine skin-adipose tissues is probably contributed by a unique micromechanical process coupled with the bulk mechanical and failure properties. Both porcine skin and adipose tissues contain substantial fibrous microstructures that are absent in synthetic polymers. For perspective, collagen fibres constitute approximately 75% of the dry fat-free mass of the skin dermis [66], and adipocytes in adipose tissue are supported by networks of collagenous structures such as the reinforced basement membrane and interlobular septa [33,67]. Therefore, it is reasonable to theorize that collagen microfibres near the crack tip play an important role in the local failure process during dynamic puncture of these tissues. This involves reversible intensification and realignment of local collagen fibres along the crack opening direction under crack expansion stresses, as revealed by mode-I fracture tests and post-mortem microscopy [44,68]. The reconfigured, highly aligned fibres can mitigate and redistribute stress concentration through non-local deformation, leading to the emergence of strong crack blunting and fibre bridging effects [44]. This creates a shielding mechanism that enhances the energy dissipation and defect/flaw tolerance of the bulk collagenous tissue compared with a single-network synthetic polymer counterpart [68]. These complex interactions between microstructures and micromechanical effects are ultimately responsible for the ductile-like failure behaviour and strong damage reduction capability of the layered porcine skin-adipose tissue during dynamic puncture, as well as its unique material properties (as described in §2), including the combination of relatively low modulus, stretchability and exceptionally high toughness. Although the characterization of collagen-fibre-mediated microstructural damage in biological tissues is beyond the scope of this work, we have observed fibre pull-out from puncture damages in both our porcine skin and adipose tissues.

Furthermore, we speculate that the compressibility of skin and adipose tissues may also play a notable role in their exceptional damage reduction capability. As theorized in Fregonese *et al.* [69], tough and compressible soft materials exhibit a higher puncture resistance than their incompressible counterpart. While a quasi-incompressibility (Poisson's ratio approx. 0.45–5) was assumed in some literature for human skin, adipose and various soft tissues [66,70–72], several studies have reported a finite bulk modulus (100 kPa to 0.1 GPa) for human muscle, skin and subcutaneous tissues [73–75].

3.2. Validation of the damage reduction theory in bilayer structures

In general, the observed enhanced resistance to dynamic puncture and rate-based damage reduction capability in both natural skin tissues and synthetic bilayer tissue simulants, compared with their substrate materials alone, can be explained by the theoretical framework of dynamic puncture energetics outlined in §1. This theoretical framework adopts a simplified bilayer structure that consists of a soft substrate layer covered by a thinner, more damage-resistant outer skin-like layer. Therefore, based on the experimental results of dynamic puncture in simple bilayer silicone tissue simulants, we provide quantitative evidence for the four key hypotheses and validate the theoretical damage reduction mechanics described in §1.

3.2.1. Effect of interlayer properties

Figure 3, combined with the material properties (μ and Γ) provided in §2, demonstrates that the incorporation of a stiffer and tougher outer layer (e.g. HRS) significantly enhances the damage reduction capability of the corresponding bilayer composite structure. The maximum depth of puncture (D_{max}) shows a significant decrease with increasing t_{out} , especially at a lower applied puncture rate ($v = 10.3 \pm 0.3 \text{ m s}^{-1}$). The relative extent of damage (D_{norm}) is reduced by approximately 50–40% across all bilayer tissue simulants and puncture conditions tested. These results are consistent with equation (1.1) and validate the hypothesis that the puncture resistance and damage reduction capability of a layered composite material are enhanced by the difference in the fracture-relevant material properties between the outer and substrate layers.

3.2.2. Effect of outer layer thickness

While figure 3 indicates an enhanced damage reduction capability in all our tested bilayer silicone tissue simulants, we note that the dependence of D_{max} and D_{norm} on t_{out} appears to be nonlinear and asymptotic as t_{out} increases from 0 to 4 mm. The change in the magnitude of D_{max} between samples with a thinner ($t_{\text{out}} = 2 \text{ mm}$) and thicker ($t_{\text{out}} = 4 \text{ mm}$) outer layer is minor compared with that between $t_{\text{out}} = 0 \text{ mm}$ and $t_{\text{out}} = 2 \text{ mm}$ and the total D_{max} , especially in the bilayer tissue simulant with a USS substrate (hollow circles; figure 3) and the one with an MRS substrate tested at a high rate (orange squares; figure 3). This behaviour is consistent with our hypothesis in §1 that the magnitude of D_{max} decreases asymptotically with increasing t_{out} and is constrained in a bilayer material.

To visualize and quantitatively validate the theory of the effect of outer layer thickness on damage reduction (D_{max} and D_{norm}), as outlined in equations (1.2) and (1.3), we present theoretical predictions of the dependence of D_{max} and D_{norm} on t_{out} in figure 3a,b, respectively. The theoretical curves are compared with the puncture experiments in the bilayer tissue simulant with an MRS substrate at $v = 10.3 \pm 0.3$ m s⁻¹ (blue squares). As detailed in the electronic supplementary material, these theoretical curves are estimated using the documented material properties (from §2) and measured fracture characteristics without data fitting. The experimental results show good agreement with the theory, with the theoretical curve approaching a lower limit corresponding to $D_{\text{max}} = 6.4$ mm or $D_{\text{norm}} = 0.69$ as t_{out} increases. This confirms that the lower limit of D_{max} is constrained by the

royalsocietypublishing.org/journal/rsif J. R. Soc. Interface 21: 20240311

material properties of the outer layer. The discrepancy between the experiments and the theory at a large $t_{\rm out}$ is probably due to the simplification of frictional dissipation (electronic supplementary material). While we assume a moderate rate-dependent effect in the theory, further validation at higher puncture rates requires an accurate mathematical description and systematic characterization of viscoelastic behaviours.

3.2.3. Effect of substrate material

While bilayer silicone samples with a USS substrate show a similar D_{norm} versus t_{out} trend in figure 2b compared with its counterpart with a stiffer MRS substrate, the former material exhibits a higher damage reduction capability, as evident from its significantly lower D_{norm} values in figure 2b at the same outer layer thickness (t_{out}) and puncture rate $(v = 10.3 \pm 0.3 \text{ m s}^{-1})$. However, in general, the USS substrate produces a slightly larger damage size (D_{max}) than the MRS substrate at the three tested values t_{out} , as shown in figure 2a. This relatively high magnitude of D_{max} is probably attributed to the low stiffness and toughness of the USS substrate material (table 1). Additionally, these properties also differ more significantly from the stiffness and toughness of the HRS outer layer compared with the difference between the MRS substrate and the HRS outer layer. Consequently, based on equation (1.2), the energy balance corresponding to an incremental increase of the thickness of the HRS outer layer (t_{out}) yields a higher reduction of D_{max} (ΔD_{max}) in the bilayer simulant with a USS substrate than in its counterpart at the same applied puncture rate. Figure 3a indicates that the magnitude of ΔD_{max} is large enough to compensate for the difference between D_{max} in the two substrate materials alone $(t_{\text{out}} = 0)$, thus resulting in a lower D_{norm} value. This validates the hypothesis of the effect of the substrate material on the damage reduction capability inferred from equation (1.4).

3.2.4. Rate-dependent damage resistance

The effect of outer layer thickness (t_{out}) on the resistance to puncture damage exhibits a strong rate dependence in bilayer silicone tissue simulants with an MRS substrate, as shown in figure 3b, and verified by statistical analysis. The sensitivity of D_{norm} to the variation in t_{out} decreases significantly (p < 0.001) as the applied puncture rate increases from $v = 10.3 \pm 0.3$ m s⁻¹ to $v = 34.4 \pm 0.8$ m s⁻¹. This rate dependence is consistent with the rate-mediated form-function relationship previously reported by Zhang & Anderson [19] in the dynamic puncture testing of similar silicone simulants, where the effect of the sharpness of the puncture tool (controlled by the cusp angle) on the depth of puncture decreases in strength as the puncture rate increases from $v \approx 10$ m s⁻¹ to $v \approx 50$ m s⁻¹. Thus, the observed rate-dependent puncture behaviour in figure 3 is probably governed by similar underlying viscoelastic mechanics related to the rate-dependent stiffening and toughening effects of the constituent silicone elastomers in the two layers [19].

Quantitative evidence from shear rheology suggests a stronger viscoelastic effect in Solaris elastomers with a lower mixing ratio (part A : part B) [41]. This, combined with figure 3, supports our hypothesis that the MRS substrate layer exhibits stronger rate dependence than the HRS outer layer. Consequently, the differences in the material properties (μ and Γ) between the MRS and HRS layers decrease at higher puncture rates. Based on the puncture energetics discussed in §1, this ultimately leads to a reduced strength of damage reduction (as characterized by D_{norm}) in the bilayer structure. At extremely high puncture rates such that the substrate and outer layers become mechanically similar, the D_{norm} versus t_{out} relationship in figure 3b is expected to approach a theoretical limit, $D_{\text{norm}} \approx 1$, as indicated by the grey dotted line. Conversely, at low to quasi-static puncture rates, the lower limit of the relationship is presumably close to the theoretical curve in figure 3. Overall, the rate-based properties of the outer and substrate layers play a substantial role in the damage reduction capability of a bilayer structure during dynamic puncture. The susceptibility of the bilayer structure to puncture damage depends on how the difference in interlayer properties is affected at higher applied puncture rates.

4. Concluding remarks

Previous studies on the mechanics of living puncture systems often focus on the form–function relationship associated with morphology of the puncture tool [19,43,55,57,76–80]. Our findings highlight the necessity of incorporating bio-relevant dynamic material response of layered skin-like material structures for a comprehensive biomechanical analysis. The tool–material interaction, energy transfer and damage creation during biological puncture are highly dependent on how the target material reacts to external loading and impact at specific dynamic rates. Therefore, generalization of the puncture performance and energetics across different biological systems requires knowledge of the rate-based mechanical and failure properties and the architectures of the constituent material layers being punctured.

Our experimental characterization using dynamic puncture with a conical tool reveals the substantial role of a thin outer layer in enhancing the damage reduction capability of bilayer composite structures, owing to its higher stiffness, toughness and larger lateral extent of damage compared with the substrate layer. The longitudinal extent of damage (D_{max}) is governed by the material properties of both layers through puncture energetics, with larger differences in energy dissipation between the two layers resulting in greater damage reduction (D_{norm}) . Moreover, our findings suggest that a layered biological structure of mammalian skin and adipose tissues may exhibit unique mechanical and failure properties during dynamic puncture, leading to remarkable puncture resistance and superior damage reduction capability compared with its synthetic tissue simulant

counterpart, despite a relatively thin skin layer. These findings offer new evidence-based insights into the universal presence and adaptation of similar animal integumentary systems as a defensive mechanism against dynamic puncture.

The unique interplay between microfibre-mediated local failure process and elasticity in layered mammalian skin tissues, coupled with large differences in the material properties and thicknesses of the outer and subcutaneous layers, allows for concurrent optimization of both damage resistance and deformability. This dual functionality is crucial for preventing biological puncture-induced damage and injuries while providing the organism with the ability to accommodate compression and blunt impact through large reversible deformation [81] and the flexibility for complex movements and locomotion. These speculations are supported by various studies on layered tissues and biological composite structures [3,4,8–10,12,82], which demonstrate enhanced strength and superior mechanical performance due to variations in constituent materials and microstructures. For example, dromedary camels can eat and swallow prickly pear cacti without internal damage due to their mesostructured keratinized papillae [82]. Elephant trunks exhibit both exceptional durability and manoeuvrability due to the hierarchical layered structure of its skin dermis with a thin keratin outer armour layer covering a bimodal network of both perpendicular and parallel arrangement of collagen fibres [12]. These layered structures can maximize organism survival and provide the animal with functional advantages in complex environments.

The rate-dependent puncture behaviours observed in our bilayer silicone tissue simulants imply that biological puncture systems can potentially compensate for suboptimal performance or expand their selection of target materials by leveraging higher puncture speeds, as observed in [19]. While preliminary dynamic puncture tests on layered porcine skin-adipose tissues using two different puncture rates ($v = 10.3 \pm 0.3$ m s⁻¹ and $v = 16.7 \pm 0.3$ m s⁻¹) showed inconclusive rate-dependent effects on the damage reduction capability (figure 2), we note that these tests were conducted at a relatively small scale, which limits the magnitude of the maximum puncture rate. Future experimental studies on larger scale samples can focus on the effect of puncture rate on the relative magnitude of the interlayer properties. We anticipate that similar rate-based puncture behaviours as observed in bilayer silicone tissue simulants will occur in biological skin tissues if the subcutaneous layer exhibits stronger strain-rate-based stiffening and toughening effects compared with the outer skin layer.

Finally, the distinct puncture failure behaviours of skin and skin-like tissues, compared with less damage-resistant synthetic polymers and composites, highlight the necessity of a theoretical framework that incorporates ductile, flaw-tolerant failure behaviours. However, existing puncture models often lack predictive power for such puncture behaviours due to their focus on low-rate and quasi-static puncture mechanics related to needle insertion or deep indentation in polymeric materials (e.g. [57,62,64,69,83–85]). To our knowledge, the mathematical framework for puncture energetics developed by Zhang & Anderson [13] is a notable exception that addresses ductile failure behaviours for dynamic biological puncture. However, generalizing this theory to layered integumentary systems requires further characterization and an improved understanding of their multi-scale failure behaviours, with the incorporation of biological composite structures, viscoelasticity and even anisotropic effects. Overall, this work represents an initial step towards unravelling the biomechanical complexity of biological puncture systems. We hope that our findings will catalyse future discussions on the mechanics of animal weapons and defensive mechanisms, with broad applications in evolutionary biomechanics, injury biomechanics and bio-inspired engineering designs.

Ethics. This work did not require ethical approval from a human subject or animal welfare committee.

Data accessibility. All data needed to evaluate the conclusions in the paper are present in the paper and/or the electronic supplementary material. Supplementary material is available online [86].

Declaration of Al use. We have not used AI-assisted technologies in creating this article.

Authors' contributions. B.Z.: conceptualization, data curation, formal analysis, investigation, methodology, validation, writing—original draft, writing—review and editing; P.S.L.A.: conceptualization, funding acquisition, project administration, supervision, writing—review and editing.

All authors gave final approval for publication and agreed to be held accountable for the work performed therein.

Conflict of interests. We declare we have no competing interests.

Funding. This work was supported by the National Science Foundation (grant NSF IOS19-42906 CAR to P.S.L.A.).

Acknowledgements. The authors thank Miranda O'Dell at the Carl R. Woese Institute for Genomic Biology of UIUC for helping with 3D printing. We also extend our thanks to the three reviewers for their constructive feedback that greatly improved this manuscript.

References

- 1. Wei JCJ, Edwards GA, Martin DJ, Huang H, Crichton ML, Kendall MAF. 2017 Allometric scaling of skin thickness, elasticity, viscoelasticity to mass for micro-medical device translation: from mice, rats, rabbits, pigs to humans. Sci. Rep. 7, 15885. (doi:10.1038/s41598-017-15830-7)
- 2. Zhu D, Ortega CF, Motamedi R, Szewciw L, Vernerey F, Barthelat F. 2012 Structure and mechanical performance of a 'modern' fish scale. *Adv. Eng. Mater.* **14**, 1–10. (doi:10.1002/adem.201180057)
- 3. Zhu D, Szewciw L, Vernerey F, Barthelat F. 2013 Puncture resistance of the scaled skin from striped bass: collective mechanisms and inspiration for new flexible armor designs. *J. Mech. Behav. Biomed. Mater.* 24, 30–40. (doi:10.1016/j.jmbbm.2013.04.011)
- 4. Wang B, Yang W, Sherman VR, Meyers MA. 2016 Pangolin armor: overlapping, structure, and mechanical properties of the keratinous scales. *Acta Biomater.* **41**, 60–74. (doi:10.1016/j.actbio.2016.05.028)
- 5. Minicozzi MR, Perez J, Kimball DS, Gibb AC. 2019 Scale thickness predicts skin puncture-force resistance in three pleuronectiform fishes. *Integr. Org. Biol.* 1, obz005. (doi:10.1093/iob/obz005)
- 6. Ghods S, Murcia S, Ossa EA, Arola D. 2019 Designed for resistance to puncture: the dynamic response of fish scales. *J. Mech. Behav. Biomed. Mater.* **90**, 451–459. (doi:10.1016/j.jmbbm.2018.10.037)

royalsocietypublishing.org/journal/rsif

J. R. Soc. Interface 21: 20240311

- 7. Lazarus BS, Velasco-Hogan A, Gómez-del Río T, Meyers MA, Jasiuk I. 2020 A review of impact resistant biological and bioinspired materials and structures. *J. Mater. Res. Technol.* **9**, 15 705–15 738. (doi:10.1016/j.jmrt.2020.10.062)
- Ghazlan A, Ngo T, Tan P, Xie YM, Tran P, Donough M. 2021 Inspiration from nature's body armours A review of biological and bioinspired composites. Comp. B Eng. 205, 108513. (doi:10.1016/j.compositesb.2020.108513)
- 2. Yaseen AA, Waqar T, Khan MAA, Asad M, Djavanroodi F. 2021 Fish scales and their biomimetic applications. Front. Mater. 8, 1. (doi:10.3389/fmats.2021.649456)
- Zolotovsky K, Varshney S, Reichert S, Arndt EM, Dao M, Boyce MC, Ortiz C. 2021 Fish-inspired flexible protective material systems with anisotropic bending stiffness. Commun. Mater.
 2, 35. (doi:10.1038/s43246-021-00140-3)
- 11. Maiorana CH, Jotawar RA, German GK. 2022 Biomechanical fracture mechanics of composite layered skin-like materials. Soft Matter 18, 2104–2112. (doi:10.1039/d1sm01187a)
- 12. Schulz AK, Plotczyk M, Sordilla S, Boyle M, Singal K, Reidenberg JS, Hu DL, Higgins CA. 2023 Second harmonic generation imaging reveals entanglement of collagen fibers in the elephant trunk skin dermis. bioRxiv. (doi:10.1101/2023.08.11.553031)
- Zhang B, Anderson PSL. 2022 Modelling biological puncture: a mathematical framework for determining the energetics and scaling. J. R. Soc. Interface 19, 20220559. (doi:10.1098/rsif.2022.0559)
- Scali M, Breedveld P, Dodou D. 2019 Experimental evaluation of a self-propelling bio-inspired needle in single- and multi-layered phantoms. Sci. Rep. 9, 19988. (doi:10.1038/s41598-019-56403-0)
- 15. Galloway KA, Porter ME. 2021 Predator-prey interactions examined using lionfish spine puncture performance. Integr. Org. Biol. 3, obaa049. (doi:10.1093/iob/obaa049)
- 16. Anderson PSL, LaCosse J, Pankow M. 2016 Point of impact: the effect of size and speed on puncture mechanics. Interface Focus 6, 20150111. (doi:10.1098/rsfs.2015.0111)
- 17. Anderson PSL. 2018 Making a point: shared mechanics underlying the diversity of biological puncture. J. Exp. Biol. 221, jeb187294. (doi:10.1242/jeb.187294)
- 18. Anderson PSL, Kawano SM. 2022 Different traits at different rates: the effects of dynamic strain rate on structural traits in biology. *Integr. Comp. Biol.* **62**, 683. (doi:10.1093/icb/icac066)
- 9. Zhang B, Anderson PSL. 2023 Investigation of the rate-mediated form-function relationship in biological puncture. Sci. Rep. 13, 12097. (doi:10.1038/s41598-023-39092-8)
- 20. Penning DA, Sawvel B, Moon BR. 2016 Debunking the viper's strike: harmless snakes kill a common assumption. Biol. Lett. 12, 20160011. (doi:10.1098/rsbl.2016.0011)
- 21. Ryerson WG, Tan W. 2017 Strike kinematics and performance in juvenile ball pythons (Python regius). J. Exp. Zool. A. Ecol. Integr. Physiol. 327, 453–457. (doi:10.1002/jez.2131)
- 22. Ryerson WG. 2020 Ontogeny of strike performance in ball pythons (*Python regius*): a three-year longitudinal study. Zoology 140, 125780. (doi:10.1016/j.zool.2020.125780)
- 23. Schulz JR, Jan I, Sangha G, Azizi E. 2019 The high speed radular prey strike of a fish-hunting cone snail. Curr. Biol. 29, R788–R789. (doi:10.1016/j.cub.2019.07.034)
- 24. Nüchter T, Benoit M, Engel U, Ozbek S, Holstein TW. 2006 Nanosecond-scale kinetics of nematocyst discharge. Curr. Biol. 16, R316–8. (doi:10.1016/j.cub.2006.03.089)
- 25. Patek SN, Baio JE, Fisher BL, Suarez AV. 2006 Multifunctionality and mechanical origins: ballistic jaw propulsion in trap-jaw ants. *Proc. Natl Acad. Sci. USA* **103**, 12 787–12 792. (doi: 10.1073/pnas.0604290103)
- 26. Zhang B, Anderson PSL. 2024 How rate-based stretchability of soft solids controls fracture morphology in dynamic conical puncture. *Int. J. Impact Eng.* **187**, 104911. (doi:10.1016/j. ijimpeng.2024.104911)
- 27. Anderson PSL, Crofts SB, Kim JT, Chamorro LP. 2019 Taking a stab at quantifying the energetics of biological puncture. Integr. Comp. Biol. 59, 1586–1596. (doi:10.1093/icb/icz078)
- 28. Shergold OA, Fleck NA, Radford D. 2006 The uniaxial stress versus strain response of pig skin and silicone rubber at low and high strain rates. *Int. J. Impact Eng.* 32, 1384–1402. (doi: 10.1016/j.ijimpeng.2004.11.010)
- 29. Khanafer K, Duprey A, Schlicht M, Berguer R. 2009 Effects of strain rate, mixing ratio, and stress-strain definition on the mechanical behavior of the polydimethylsiloxane (PDMS) material as related to its biological applications. *Biomed. Microdevices* 11, 503–508. (doi:10.1007/s10544-008-9256-6)
- 30. Guo L, Lv Y, Deng Z, Wang Y, Zan X. 2016 Tension testing of silicone rubber at high strain rates. Polym. Test. 50, 270—275. (doi:10.1016/j.polymertesting.2016.01.021)
- 31. Creton C, Ciccotti M. 2016 Fracture and adhesion of soft materials: a review. Rep. Prog. Phys. 79, 046601. (doi:10.1088/0034-4885/79/4/046601)
- 32. Meng Y, Xu W, Newman MR, Benoit DSW, Anthamatten M. 2019 Thermoreversible siloxane networks: soft biomaterials with widely tunable viscoelasticity. *Adv. Funct. Mater.* 29, 1. (doi:10.1002/adfm.201903721)
- 33. Comley K, Fleck N. 2012 The compressive response of porcine adipose tissue from low to high strain rate. Int. J. Impact Eng. 46, 1–10. (doi:10.1016/j.ijimpeng.2011.12.009)
- 34. Purslow PP. 1983 Measurement of the fracture toughness of extensible connective tissues. J. Mater. Sci. 18, 3591–3598. (doi:10.1007/BF00540731)
- 35. Lim J, Hong J, Chen WW, Weerasooriya T. 2011 Mechanical response of pig skin under dynamic tensile loading. *Int. J. Impact Eng.* **38**, 130–135. (doi:10.1016/j.ijimpeng.2010.09. 003)
- 36. Wong WLE, Joyce TJ, Goh KL. 2016 Resolving the viscoelasticity and anisotropy dependence of the mechanical properties of skin from a porcine model. *Biomech. Model. Mechanobiol.* **15**, 433–446. (doi:10.1007/s10237-015-0700-2)
- 37. Tirella A, Mattei G, Ahluwalia A. 2014 Strain rate viscoelastic analysis of soft and highly hydrated biomaterials. J. Biomed. Mater. Res. A. 102, 3352–3360. (doi:10.1002/jbm.a.34914)
- 38. Gidde RR, Pawar PM. 2017 On effect of viscoelastic characteristics of polymers on performance of micropump. Adv. Mech. Eng. 9, 168781401769121. (doi:10.1177/1687814017691211)
- 39. Zhang B, Shiang CS, Yang SJ, Hutchens SB. 2019 Y-shaped cutting for the systematic characterization of cutting and tearing. Exp. Mech. 59, 517–529. (doi:10.1007/s11340-019-00479-2)
- 40. Chen L, Lin S, Deng P, Wang X. 2019 Microdrop impact on soft substrates at low Weber numbers. J. Adhes. Sci. Technol. 33, 2128–2140. (doi:10.1080/01694243.2019.1632048)
- 41. Darby DR, Cai Z, Mason CR, Pham JT. 2022 Modulus and adhesion of Sylgard 184, Solaris, and Ecoflex 00-30 silicone elastomers with varied mixing ratios. *J. Appl. Polym. Sci.* 139, 1. (doi:10.1002/app.52412)
- 42. Glover JD, McLaughlin CE, McFarland MK, Pham JT. 2020 Extracting uncrosslinked material from low modulus Sylgard 184 and the effect on mechanical properties. *J. Polym. Sci. A.* **58**, 343–351. (doi:10.1002/pol.20190032)
- 43. Zhang B, Hutchens SB. 2021 On the relationship between cutting and tearing in soft elastic solids. Soft Matter 17, 6728–6741. (doi:10.1039/d1sm00527h)
- 44. Pissarenko A, Yang W, Quan H, Poyer B, Williams A, Brown KA, Meyers MA. 2020 The toughness of porcine skin: quantitative measurements and microstructural characterization. *J. Mech. Behav. Biomed. Mater.* **109**, 103848. (doi:10.1016/j.jmbbm.2020.103848)
- 45. Cesa CM, Kirchgessner N, Mayer D, Schwarz US, Hoffmann B, Merkel R. 2007 Micropatterned silicone elastomer substrates for high resolution analysis of cellular force patterns. *Rev. Sci. Instrum.* **78**, 034301. (doi:10.1063/1.2712870)
- 46. Lee J et al. 2022 An artificial tactile neuron enabling spiking representation of stiffness and disease diagnosis. Adv. Mater. Weinheim 34. (doi:10.1002/adma.202201608)
- Geerligs M, Peters GWM, Ackermans PAJ, Oomens CWJ, Baaijens FPT. 2008 Linear viscoelastic behavior of subcutaneous adipose tissue. Biorheology 45, 677–688. (doi:10.3233/BIR-2008-0517)
- 48. Comley K, Fleck NA. 2010 The toughness of adipose tissue: measurements and physical basis. J. Biomech. 43, 1823-1826. (doi:10.1016/j.jbiomech.2010.02.029)

royalsocietypublishing.org/journal/rsif

J. R. Soc. Interface 21: 20240311

- 49. Comley K, Fleck N. 2009 The mechanical response of porcine adipose tissue. ASME J. Biomech. Eng. 1. (doi:10.1016/j.ijimpeng.2011.12.009)
- 50. Fenton LA, Horsfall I, Carr DJ. 2020 Skin and skin simulants. Aust. J. Forensic Sci. 52, 96–106. (doi:10.1080/00450618.2018.1450896)
- 51. Shergold OA, Fleck NA. 2005 Experimental investigation into the deep penetration of soft solids by sharp and blunt punches, with application to the piercing of skin. *J. Biomech. Eng.* 127, 838–848. (doi:10.1115/1.1992528)
- 52. Singh G, Gupta V, Chanda A. 2022 Artificial skin with varying biomechanical properties. Mater. Today 62, 3162–3166. (doi:10.1016/j.matpr.2022.03.433)
- 53. Sun Z, Gepner BD, Cottler PS, Lee SH, Kerrigan JR. 2021 In vitro mechanical characterization and modeling of subcutaneous adipose tissue: a comprehensive review. *J. Biomech. Eng.* **143**, 1. (doi:10.1115/1.4050286)
- 54. Zhang B. 2021 Y-shaped cutting as a characterization method for the failure of soft elastic solids. PhD dissertation, University of Illinois Urbana-Champaign, Urbana, IL.
- 55. Schofield RMS, Choi S, Coon JJ, Goggans MS, Kreisman TF, Silver DM, Nesson MH. 2016 Is fracture a bigger problem for smaller animals? Force and fracture scaling for a simple model of cutting, puncture and crushing. *Interface Focus* 6, 20160002. (doi:10.1098/rsfs.2016.0002)
- 56. Bar-On B. 2019 On the form and bio-mechanics of venom-injection elements. Acta Biomater. 85, 263–271. (doi:10.1016/j.actbio.2018.12.030)
- 57. Kundanati L, Guarino R, Menegon M, Pugno NM. 2020 Mechanics of snake biting: experiments and modelling. *J. Mech. Behav. Biomed. Mater.* **112**, 104020. (doi:10.1016/j.jmbbm. 2020.104020)
- 58. Jensen KH, Knoblauch J, Christensen AH, Haaning KS, Park K. 2020 Universal elastic mechanism for stinger design. Nat. Phys. 16, 1074–1078. (doi:10.1038/s41567-020-0930-9)
- 59. Bar-On B. 2023 The effect of structural curvature on the load-bearing characteristics of biomechanical elements. *J. Mech. Behav. Biomed. Mater.* **138**, 105569. (doi:10.1016/j.jmbbm.2022.105569)
- 60. Quan H, Liang X, Zhang X, Meyers MA, McMeeking RM, Arzt E. 2024 The shape of nature's stingers revealed. *Proc. Natl Acad. Sci. USA* 121, e2316320121. (doi:10.1073/pnas. 2316320121)
- 61. Evans AR et al. 2021 A universal power law for modelling the growth and form of teeth, claws, horns, thorns, beaks, and shells. BMC Biol. 19, 58. (doi:10.1186/s12915-021-00990-w)
- 62. Fregonese S, Bacca M. 2022 How friction and adhesion affect the mechanics of deep penetration in soft solids. Soft Matter 18, 6882–6887. (doi:10.1039/d2sm00638c)
- 63. Montanari M, Spagnoli A. 2024 Exploring the influence of friction in the puncture mechanics of soft solids. Meccanica (doi:10.1007/s11012-024-01767-5)
- 64. Shergold OA, Fleck NA. 2004 Mechanisms of deep penetration of soft solids, with application to the injection and wounding of skin. *Proc. R. Soc. Lond. A.* 460, 3037–3058. (doi:10.1098/rspa.2004.1315)
- 65. Hui CY, A. J, Bennison SJ, Londono JD. 2003 Crack blunting and the strength of soft elastic solids. Proc. R. Soc. Lond. A. 459, 1489–1516. (doi:10.1098/rspa.2002.1057)
- 66. Joodaki H, Panzer MB. 2018 Skin mechanical properties and modeling: a review. Proceedings of the institution of mechanical engineers. J. Eng. Med. 232, 323–343. (doi:10.1177/0954411918759801)
- 67. Comley K, Fleck NA. 2010 A micromechanical model for the Young's modulus of adipose tissue. Int. J. Solids Struct. 47, 2982—2990. (doi:10.1016/j.ijsolstr.2010.07.001)
- 68. Bircher K, Zündel M, Pensalfini M, Ehret AE, Mazza E. 2019 Tear resistance of soft collagenous tissues. Nat. Commun. 10, 792. (doi:10.1038/s41467-019-08723-y)
- 69. Fregonese S, Tong Z, Wang S, Bacca M. 2023 Theoretical puncture mechanics of soft compressible solids. J. Appl. Mech. 90, 1. (doi:10.1115/1.4062844)
- 70. Ou H, Zhan P, Kang L, Su J, Hu X, Johnson S. 2018 Region-specific constitutive modeling of the plantar soft tissue. *Biomech. Model. Mechanobiol.* 17, 1373–1388. (doi:10.1007/s10237-018-1032-9)
- 71. Naseri H, Iraeus J, Johansson H. 2020 The effect of adipose tissue material properties on the lap belt-pelvis interaction: a global sensitivity analysis. *J. Mech. Behav. Biomed. Mater.* **107**, 103739. (doi:10.1016/j.jmbbm.2020.103739)
- 72. Singh G, Chanda A. 2021 Mechanical properties of whole-body soft human tissues: a review. Biomed. Mater. 16, 062004. (doi:10.1088/1748-605X/ac2b7a)
- 73. Saraf H, Ramesh KT, Lennon AM, Merkle AC, Roberts JC. 2007 Mechanical properties of soft human tissues under dynamic loading. *J. Biomech.* **40**, 1960–1967. (doi:10.1016/j.jbiomech.2006.09.021)
- 74. Thomsen M, Hernandez-Garcia A, Mathiesen J, Poulsen M, Sørensen DN, Tarnow L, Feidenhans'l R. 2014 Model study of the pressure build-up during subcutaneous injection. *PLoS One* **9**, e104054. (doi:10.1371/journal.pone.0104054)
- 75. Then C, Voql TJ, Silber G. 2012 Method for characterizing viscoelasticity of human gluteal tissue. J. Biomech. 45, 1252–1258. (doi:10.1016/j.jbiomech.2012.01.037)
- 76. Freeman PW, Lemen CA. 2007 The trade-off between tooth strength and tooth penetration: predicting optimal shape of canine teeth. *J. Zool.* **273**, 273–280. (doi:10.1111/j.1469-7998.2007.00325.x)
- 77. Crofts SB, Anderson PSL. 2018 The influence of cactus spine surface structure on puncture performance and anchoring ability is tuned for ecology. *Proc. R. Soc. B* **285**, 20182280. (doi:10.1098/rspb.2018.2280)
- 78. Das R, Yadav RN, Sihota P, Uniyal P, Kumar N, Bhushan B. 2018 Biomechanical evaluation of wasp and honeybee stingers. Sci. Rep. 8, 14945. (doi:10.1038/s41598-018-33386-y)
- Crofts SB, Lai Y, Hu Y, Anderson PSL. 2019 How do morphological sharpness measures relate to puncture performance in viperid snake fangs? Biol. Lett. 15, 20180905. (doi:10.1098/rsbl.2018.0905)
- 80. Shea-Vantine CS, Galloway KA, Ingle DN, Porter ME, Kajiura SM. 2021 Caudal spine morphology and puncture performance of two coastal stingrays. *Integr. Comp. Biol.* 61, 749–758. (doi:10.1093/jcb/jcab077)
- 81. Box F, Jacquemot C, Adda-Bedia M, Vella D. 2020 Cloaking by coating: how effectively does a thin, stiff coating hide a soft substrate? *Soft Matter* **16**, 4574–4583. (doi:10.1039/c9sm02511a)
- 82. Abou-Elhamd AS, Abd-Elkareem M, El-Zuhry Zayed A. 2018 Morphogenesis of lingual papillae of one-humped camel (*Camelus dromedarius*) during prenatal life: a light and scanning electron microscopic study. *Anat. Histol. Embryol.* 47, 38–45. (doi:10.1111/ahe.12321)
- 83. Fakhouri S, Hutchens SB, Crosby AJ. 2015 Puncture mechanics of soft solids. Soft Matter 11, 4723–4730. (doi:10.1039/c5sm00230c)
- 84. Fregonese S, Bacca M. 2021 Piercing soft solids: a mechanical theory for needle insertion. J. Mech. Phys. Solids 154, 104497. (doi:10.1016/j.jmps.2021.104497)
- 85. Montanari M, Brighenti R, Terzano M, Spagnoli A. 2023 Puncturing of soft tissues: experimental and fracture mechanics-based study. *Soft Matter* **19**, 3629–3639. (doi:10.1039/d3sm00011g)
- 86. Zhang B, Baskota B, Anderson PSL. 2024 Supplementary material from: Being thin-skinned can still reduce damage from dynamic puncture. Figshare. (doi:10.6084/m9.figshare.c. 7443052)